



Article

Bone Remodeling Process Based on Hydrostatic and Deviatoric Strain Mechano-Sensing

Natalia Branecka ¹ , Mustafa Erden Yildizdag ^{2,3} , Alessandro Ciallella ^{2,4} and Ivan Giorgio ^{2,4,*}

¹ Faculty of Mechanical and Industrial Engineering, Warsaw University of Technology, 00-661 Warsaw, Poland; natalia.branecka.dokt@pw.edu.pl

² International Research Center for the Mathematics and Mechanics of Complex Systems, University of L'Aquila, 67100 L'Aquila, Italy; yildizdag@itu.edu.tr (M.E.Y.); alessandro.ciallella@univaq.it (A.C.)

³ Faculty of Naval Architecture and Ocean Engineering, Istanbul Technical University, Istanbul 34469, Turkey

⁴ Dipartimento di Ingegneria Civile, Edile-Architettura e Ambientale (DICEAA), University of L'Aquila, 67100 L'Aquila, Italy

* Correspondence: ivan.giorgio@univaq.it

Abstract: A macroscopic continuum model intended to provide predictions for the remodeling process occurring in bone tissue is proposed. Specifically, we consider a formulation in which two characteristic stiffnesses, namely the bulk and shear moduli, evolve independently to adapt the hydrostatic and deviatoric response of the bone tissue to environmental changes. The formulation is deliberately simplified, aiming at constituting a preliminary step toward a more comprehensive modeling approach. The evolutive process for describing the functional adaptation of the two stiffnesses is proposed based on an energetic argument. Numerical experiments reveal that it is possible to model the bone remodeling process with a different evolution for more than one material parameter, as usually done. Moreover, the results motivate further investigations into the subject.

Keywords: bone remodeling; mechanical stimuli; mechano-sensing; strain energy density; hydrostatic strain; deviatoric strain



Citation: Branecka, N.; Yildizdag, M.E.; Ciallella, A.; Giorgio, I. Bone Remodeling Process Based on Hydrostatic and Deviatoric Strain Mechano-Sensing. *Biomimetics* **2022**, *7*, 59. <https://doi.org/10.3390/biomimetics7020059>

Academic Editor: Thomas Speck

Received: 27 March 2022

Accepted: 3 May 2022

Published: 6 May 2022

Publisher's Note: MDPI stays neutral with regard to jurisdictional claims in published maps and institutional affiliations.



Copyright: © 2022 by the authors. Licensee MDPI, Basel, Switzerland. This article is an open access article distributed under the terms and conditions of the Creative Commons Attribution (CC BY) license (<https://creativecommons.org/licenses/by/4.0/>).

1. Introduction

The most important tasks of the skeleton include the protection of internal organs, supporting the entire body, and acting as the leveraging organ that enables mobility. Its main component is bone tissue, a type of hard connective tissue. The shaft of the long bones and the exterior layers of the flat bones constitute the cortical bone that carries the mechanical loads for the most part. The internal tissue of skeletal bone is called trabecular bone, and it is much more porous and flexible. Bone adapts to environmental conditions responding to changes in mechanical and biochemical stimuli. In this paper, we present a mathematical model whose task is to describe the influence of mechanical loads on bone remodeling, taking into account the interplay of the biological and mechanical reactions of tissue at a macroscopic level of description.

Bone continuously adjusts to external mechanical loads, changing its properties through to the remodeling process. Bone adaptation is based on the sensing of mechanical loads and the continuous reconstruction of the bone architecture through the formation and resorption of bone tissue in a process that is influenced by external loads [1]. Mechanotransduction is the action of converting mechanical responses provided by external interactions into biochemical signals, which may induce the response of bone cells responsible for the synthesis or resorption of bone tissue. The cells in charge of this process of transducing, called osteocytes, are identified to be mechano-sensors, which detect mechanical signals and initiate and control the process of remodeling [2–4]. Osteocytes are regularly embedded in cavities of the bone matrix in hollow lacunae linked by narrow canals (see Figure 1). They form a network called the lacuno-canalicular network (OLCN) of processes that allows them to communicate with each other [5–9].

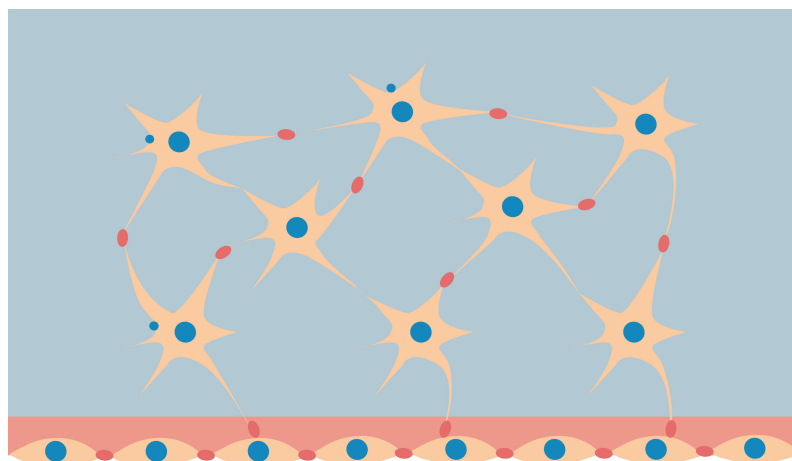


Figure 1. Osteocytes in bone matrix (star-shaped) with the formed OLCN connected to osteoblasts on the boundary.

Interconnected cells can communicate via gap junctions, which permit the diffusion of ions, metabolites, and small signaling molecules from cell to cell. Gap junctions are located in the cell membranes of all bone cells, especially in actor cells, osteocytes, and osteoblasts and at the tip of osteocyte dendritic processes [2,10].

Mechanosensation of osteocytes includes a few types of loading, above all whole tissue strain, hydrostatic pressure, and streaming potentials generated by bone fluid flow through a charged bone matrix [4]. Owing to *in vitro* experiments, it is known that osteocytes are much more sensitive to fluid shear stresses than substantial fluid pressure [7]. The osteocyte is derived from the osteoblast, but osteocytes are much more responsive and more sensitive to shear stress [11–13]. When bone is under mechanical loading, the deformation of the bone matrix generates fluid flow in the OLCN, which induces shear stress along osteocyte membranes [14–16]. Due to the different sensitivity of sensor cells to pressure and shear stress, it seems more realistic to distinguish these processes in mathematical modeling. As a matter of fact, the mechanisms involved in the sensing function of the bone tissue mechanical state are distinct and located in different sites of the osteocytes; therefore, considering them in the same way is excessively simplistic.

The role of osteocytes is to send a proper signal to activate precursor cells [5], which will trigger the generation, as required, of actor cells, that is osteoblasts or osteoclasts. Osteoblasts and osteoclasts are bone cells directly responsible for bone remodeling in the case of microdamage, replacement of old bone with new bone, and bone adaptation [17–20]. Osteoblasts are adapted to cause bone formation and osteoclasts for bone resorption; it is hypothesized that they collect different types of biochemical signals, and their activity depends on the intensity. The entire process related to intercellular communication is not fully explained and needs ulterior investigations.

There are many theoretical models based on simplified assumptions. The problem of bone adaptation and remodeling has been considered since Wolff's observations in 1892 that mathematical laws can describe changes in the architecture of bones [21,22]. Many mathematical models have been developed [23–29] dependent on various mechanical stimuli inducing bone adaptation. Among them can be mentioned diverse instances based on strain energy density [30,31], tissue damage [32–34], daily stress stimulus [35], effective stress [36], and strain [37]. In this paper, we follow the path of numerical models, where the assumption is made that bone mass adjusts in response to energy considerations, in which the loading history and energy transfers can be included [38,39]. The strain energy density (SED) is used as a control variable enabling defining the shape or bone density adaptations due to functional requirements [39,40]. A slightly different approach can be found in papers [40–46], where the classical proportional integral derivative (PID) control was employed to describe the mass density optimization macroscopically due to the remodeling process based on the feedback variable SED. Herein, we generalize the

description of the bone evolution, by including two evolutive laws on the bulk and shear moduli, in order to focus on the bone remodeling responses arising from hydrostatic and deviatoric loadings. The main idea behind the paper is to explore the simplified case of isotropic bone tissue as a preliminary step to move forward with the more realistic case of anisotropic or orthotropic tissue. In these last cases, we have to deal with many material parameters; therefore, understanding what occurs in the case of two evolving material parameters appears crucial in developing a helpful model for accurately describing the remodeling process.

2. Materials and Methods

In this study, for the sake of simplicity, bone is assumed to be an isotropic elastic material. We can formulate Hooke's law to define the stress tensor σ_{ij} as a linear combination of the volumetric and deviatoric strain tensors:

$$\sigma_{ij} = 3K \left(\frac{1}{3} \varepsilon_{kk} \delta_{ij} \right) + 2G \left(\varepsilon_{ij} - \frac{1}{3} \varepsilon_{kk} \delta_{ij} \right) \quad (1)$$

where K is the bulk modulus and G is the shear modulus. From Equation (1), it is possible then to recognize the two contributions to the stress, namely the hydrostatic:

$$\sigma^h_{ij} = 3K \left(\frac{1}{3} \varepsilon_{kk} \delta_{ij} \right) \quad (2)$$

and shear or deviatoric part:

$$\sigma^s_{ij} = 2G \left(\varepsilon_{ij} - \frac{1}{3} \varepsilon_{kk} \delta_{ij} \right) \quad (3)$$

This formulation can be generalized by using mechanical micromorphic [47–56], micropolar [57–60], higher-order [61–70], or peridynamic [71–74] models. As an opening move, the stiffnesses can be evaluated starting with the knowledge of the engineering parameters, Young's modulus Y , and Poisson's ratio ν as follows:

$$K = \frac{Y}{3(1-2\nu)} \quad (4)$$

$$G = \frac{Y}{2(1+\nu)} \quad (5)$$

since they are more straightforward to retrieve in the literature. The components of the strain tensor, in the linear approximation, can be written as:

$$\varepsilon_{ij} = \frac{1}{2} (u_{i,j} + u_{j,i}) \quad (6)$$

The index after the comma stands for the differentiation with respect to the corresponding space variable. Based on that, we can find the equations describing the strain energy density decomposed into a component associated with the hydrostatic part of the load and deviatoric one:

$$W = W_h + W_d \quad (7)$$

We remark that the decomposition of the energy in these two portions is quite convenient to use in the evolution of the stiffnesses since they are energetically orthogonal. As a matter of fact, they are devoid of any mutual coupling. For our investigation, we consider a 2D case, and specifically, the hydrostatic contribution is

$$W_h = \frac{1}{2} K (\varepsilon_{11} + \varepsilon_{22})^2 \quad (8)$$

while the deviatoric part is

$$W_d = G \left[\varepsilon_{11}^2 + \varepsilon_{22}^2 + 2\varepsilon_{12}^2 - \frac{1}{2}(\varepsilon_{11} + \varepsilon_{22})^2 \right] \tag{9}$$

We implement this way of representing the strain energy density for the problem of mechanically loaded bone. The bodies in charge of sensing mechanical loads, i.e., osteocytes, are assumed to be regularly distributed in the tissue volume. This simplifying hypothesis can be easily generalized by introducing an inhomogeneous density of osteocytes (see, e.g., [31]). However, in this work, we refrain from introducing this feature since, locally, we can safely assume that the change in the number of osteocytes is not quickly variable in the space. Osteocytes transform a mechanical signal into a biochemical one, which is, in our simplified model, instantaneously transmitted, and its intensity decays exponentially as the distance from the osteocytes (the source of the signal) increases [31,75,76]. Therefore, we consider an influence radius surrounding the osteocytes, i.e., D , and in our example, we set for it the value 0.1 mm. In the 2D example, we can write the normalized distance from a sensor cell, thought to be located in X_0 , to a given material particle in which the actor cells, namely osteoclasts and osteoblasts, act as:

$$E_s = \frac{\|X - X_0\|}{D} \tag{10}$$

The biochemical signal transmitted by osteocytes triggers the activities of the actor cells, i.e., osteoblasts and osteoclasts, in the process of bone adaptation to mechanical stimulation. According to the previous partition into hydrostatic and deviatoric parts, we can postulate the biochemical stimuli to be:

$$S_K(X, t) = \int_{\Omega} W_h(X_0, t) e^{-E_s(X, X_0)} dX_0 - S_{K0}(X, t) \tag{11}$$

$$S_G(X, t) = \int_{\Omega} W_d(X_0, t) e^{-E_s(X, X_0)} dX_0 - S_{G0}(X, t) \tag{12}$$

The osteocytes are mechanoreceptor, i.e., sensing components that monitor and respond to mechanical changes in the environment. In particular, we assume that osteocytes transmit a biochemical signal that is proportional to the elemental strain energy of the volume particle in which they are located. When formulating the evolutionary equations, we link the change in material parameters K and G occurring in time with the signal transmitted to a given elementary volume of the material. The two quantities S_{K0} and S_{G0} represent the optimal functioning conditions from a mechanical viewpoint of the bone tissue. They define homeostasis, which is the state of steady internal, mechanical conditions that should be maintained by the living system, i.e., bone tissue, to guarantee its correct functionality. In other words, homeostasis is determined by a natural resistance to change when the biological system is already in the optimal condition. The primary purpose of the bone tissue is of a mechanical nature, and it is well known that the strength of materials is differently affected by hydrostatic and deviatoric deformations or stress. One could specifically think of the von Mises yield criterion based on maximum distortion energy attainable in the material, namely the maximal deviatoric part of the deformation/stress. This simple observation leads us to think that, in principle, these two quantities S_{K0} and S_{G0} are, in fact, different. Moreover, thinking about this functional aspect, it is no coincidence that the deviatoric part, related to S_{G0} , has a predominant role.

In this formulation, since the density of osteocytes is assumed to be uniformly distributed over the considered domain, we do not introduce a function representing the number of sensor cells per unit volume as a multiplicative factor to the energy density

for the sake of simplicity, as done in [31] instead. In detail, the evolution laws for the two stiffnesses are assumed to be:

$$\frac{\partial K(S_K, t)}{\partial t} = A_K(S_K)H\left(\frac{K}{K_{Max}}\right) \tag{13}$$

$$\frac{\partial G(S_G, t)}{\partial t} = A_G(S_G)H\left(\frac{G}{G_{Max}}\right) \tag{14}$$

where the functions A_K and A_G are piecewise linear functions of the stimuli (11) and (12) as specified below:

$$A_K(S_K) = \begin{cases} r_{sK} S_K & \text{for } S_K \geq 0 \\ r_{rK} S_K & \text{for } S_K < 0 \end{cases} \tag{15}$$

and

$$A_G(S_G) = \begin{cases} r_{sG} S_G & \text{for } S_G \geq 0 \\ r_{rG} S_G & \text{for } S_G < 0 \end{cases} \tag{16}$$

The function $H(x)$ is a weight for numerical calculation that prevents the complete vanishing, as well as unlimited growth of parameters K and G and is considered to be:

$$H(x) = 4x(1 - x) \tag{17}$$

in the interval $[0, 1]$, while it is set to zero outside. The limit coefficients K_{Max} and G_{Max} represent the maximum values attainable for K and G , respectively.

When the signal is within a certain range, even in the presence of a stimulus beyond the threshold, there is no actor cell activity [31] (see Figure 2). Ratios r_{sK} , r_{rK} , r_{sG} , and r_{rG} are determined experimentally and are regulating factors. Ratio r_{sK} scales the function S_K when it is greater than or equal to 0; ratio r_{rK} scales the function S_K when it is smaller than 0, similar in the case of r_{sG} , which scales the function S_G when it is greater than or equal to 0; ratio r_{rG} scales the function S_G when it is smaller than 0. The bone remodeling process depends on mechanical stimulus intensity: when it is too low, bone is reabsorbed; when it is too high, it causes damage, but there are also optimal zones where the bone is adapting its properties to external mechanical conditions [30,40].

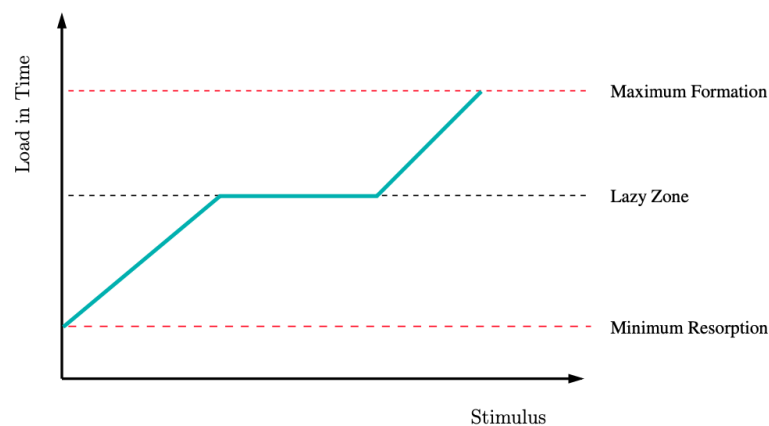


Figure 2. Effect of the load on stimulus. Low mechanical loading results in bone resorption: it is the resorption stimulus zone; subsequently, in the lazy zone (black dotted line), there is no change in bone; with a sufficiently high load, the formation of the stimulus zone occurs in a certain range highlighted with red dotted lines.

In line with the assumption that strain energy is divided into the hydrostatic and deviatoric parts, in what follows, we can observe the impact that different kinds of mechanical loading have on bone remodeling through several numerical simulations.

3. Results

The numerical computations were performed on a 2D isotropic material with the initial values presented in Table 1. By following the schema of the process shown in Figure 3, an FE algorithm was written in Comsol Multiphysics in order to test and support the hypotheses behind our model, showcasing some plausible responses that can be compared at least preliminarily and qualitatively with real-life evolutions.

Table 1. Parameters used in the numerical simulations.

| Parameter | Value |
|-----------|---|
| Y_0 | 18 GPa |
| ν_0 | 0.3 |
| D | 0.1 mm |
| K_{Max} | 30 GPa |
| G_{Max} | 13.84 GPa |
| S_{K0} | 0.001 N |
| S_{G0} | 0.001 N |
| r_{sK} | $1 \times 10^7 \text{ m}^{-3} \text{ s}^{-1}$ |
| r_{rK} | $1 \times 10^9 \text{ m}^{-3} \text{ s}^{-1}$ |
| r_{sG} | $1 \times 10^3 \text{ m}^{-3} \text{ s}^{-1}$ |
| r_{rG} | $1 \times 10^9 \text{ m}^{-3} \text{ s}^{-1}$ |

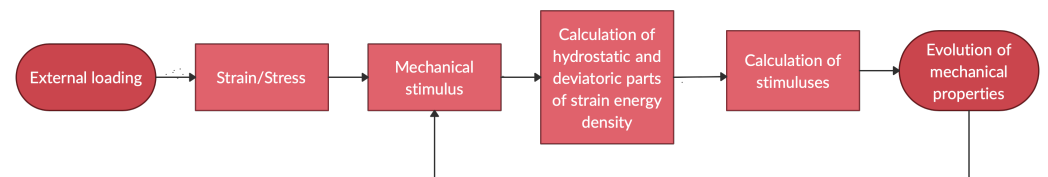


Figure 3. Flow chart of processes.

To illustrate the main feature of the proposed model, we simulated the evolution of several representative cases: two examples in which the external loads activate a pure hydrostatic and pure shear deformation, then a third case, where the two kinds of deformation are simultaneously present.

At first, we implemented the pure hydrostatic case, where a semicircular piece of bone, attached to the ground to avoid any rigid motion, but free to deform, was subjected to a distributed force perpendicular to its circular boundary (see Figure 4a).

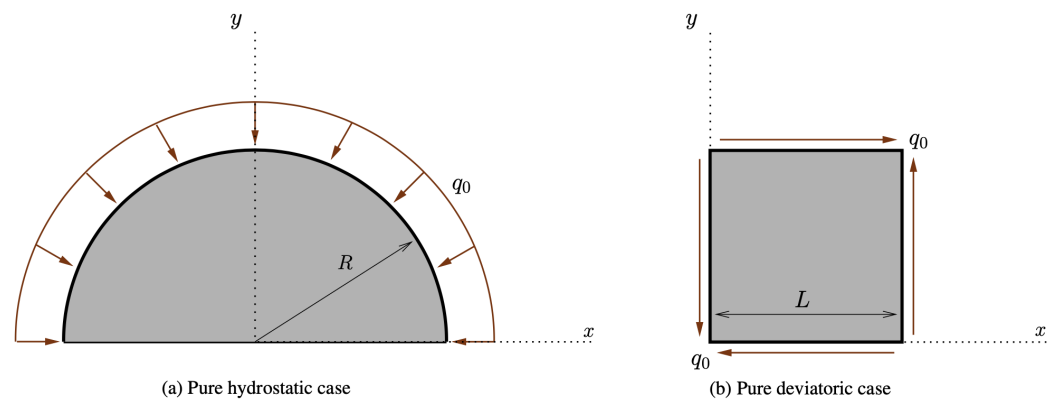


Figure 4. Schematics for the considered pure hydrostatic and pure deviatoric cases.

In particular, the maximum diameter is linked to the ground with a perfect constraint in the vertical direction and with a weak elastic potential in the other direction to prevent rigid motion horizontally and allow deformation in that direction. Figure 5 clearly exhibits the orthogonal feature of the two energy contributions. As a matter of fact, due to the

circular symmetry of the external load, also the deformation keeps this symmetry. As a consequence, no deformation involving a change of shape is activated.

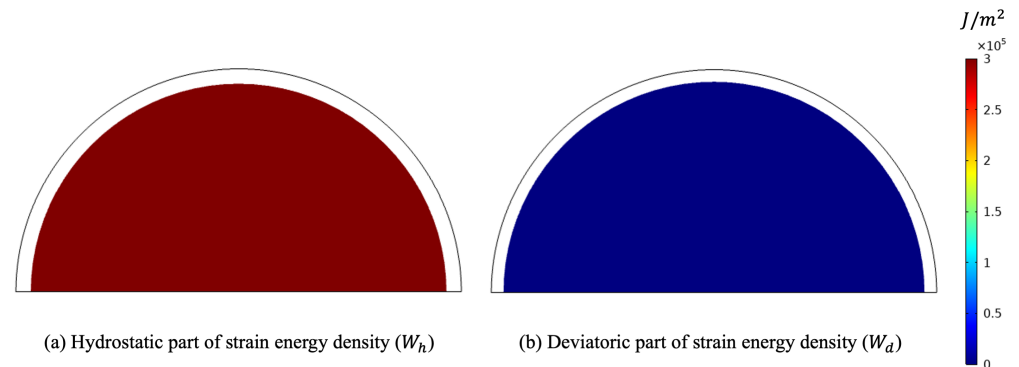
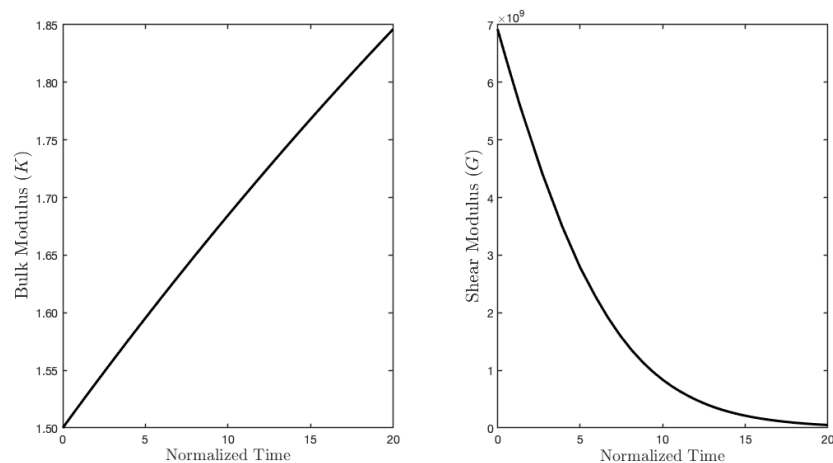
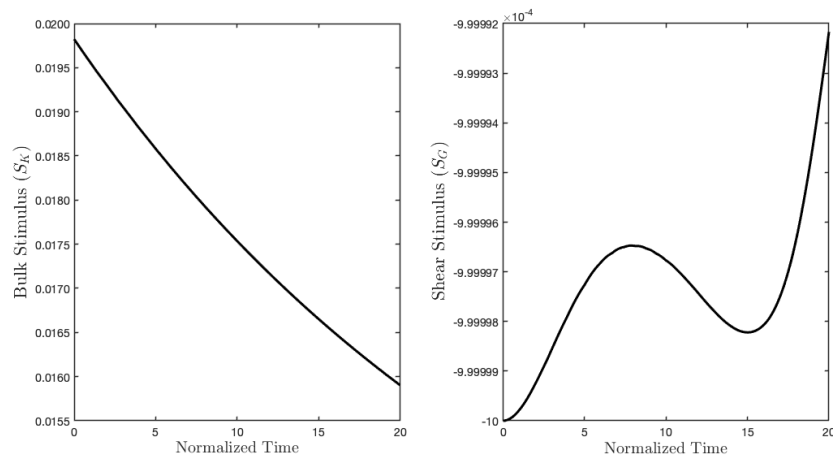


Figure 5. Deformed shape for the pure hydrostatic case (plots were obtained with a scale factor of 20).

As we expected, the parameter K , during the evolution subject to such a mechanical load, denoted by q_0 , increased due to a sufficiently high level of external action, which, in turn, produced a positive stimulus for this parameter. On the contrary, since the energy contribution of the deviatoric part is null, the related stimulus was negative, and therefore, the shear modulus started to fade (see Figure 6).



(a) Evolution of the bulk and shear moduli, expressed in Pa.



(b) Evolution of the bulk and shear stimulus, expressed in N.

Figure 6. Evolution of moduli and stimuli in time for the purely hydrostatic case.

Subsequently, we simulated the pure shear strain example (see Figure 4b). In this case, the external actions were conceived of to impose a deformation with a change of shape, but not of the area (see Figure 7). In contrast with the previous case, now, the two parameters G and K exchanged their role (see Figure 8). Indeed, K decreased because the related stimulus became negative (no hydrostatic energy was activated), while G increased for the external action, denoted by q_0 , producing a positive stimulus.

Naturally, the evolution of K and G depends on the ratios r_{sK} , r_{rK} , r_{sG} , and r_{rG} , which are to be determined by comparison with experimental tests on living bone tissues.

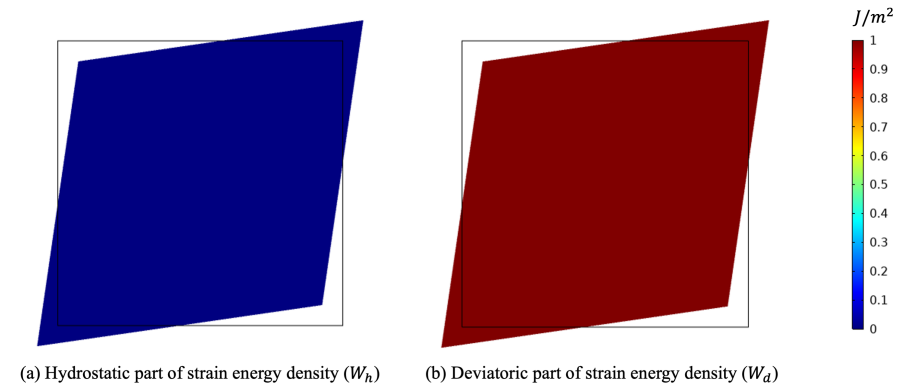


Figure 7. Deformed shape for the pure deviatoric case (plots were obtained with a scale factor of 20).

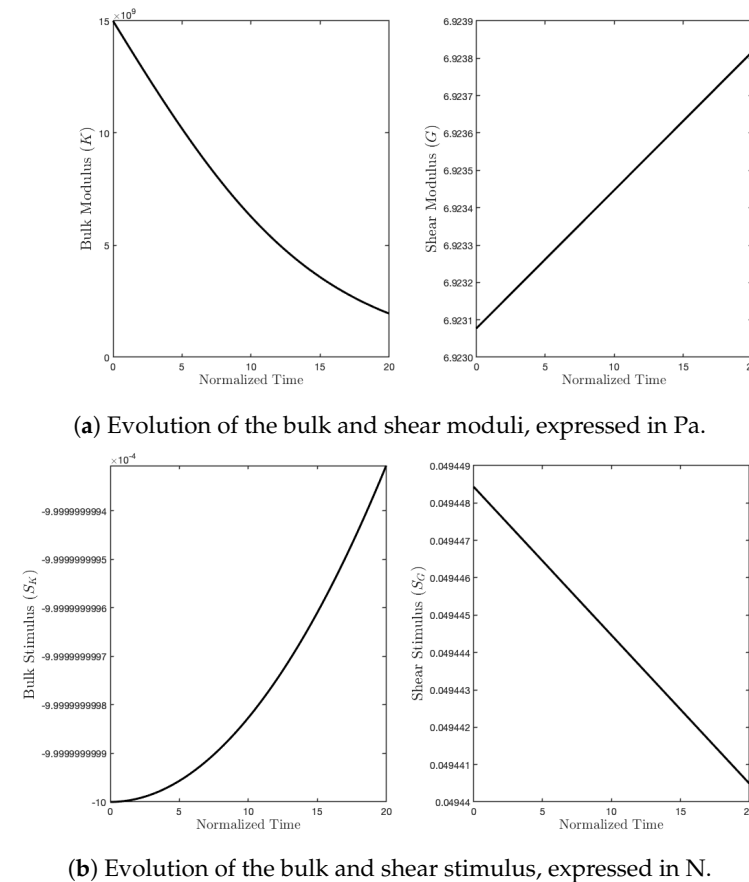


Figure 8. Evolution of moduli and stimuli in time for the purely deviatoric case.

Finally, we performed one simulation with a tensile test (see Figure 9). In this last example, both contributions of the energy were activated (see Figure 10). Here, both stimuli turned out to be positive, and hence, both stiffness parameters increased (see Figure 11).

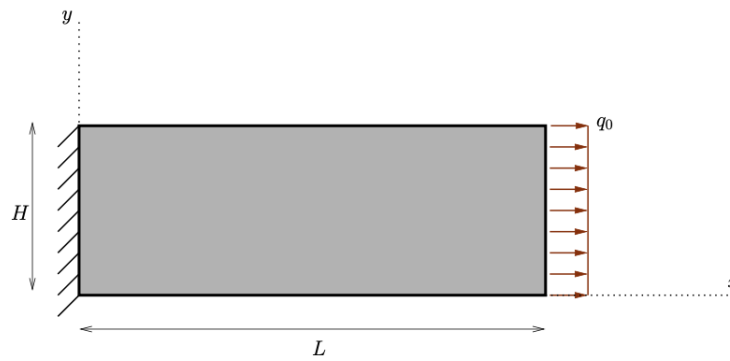
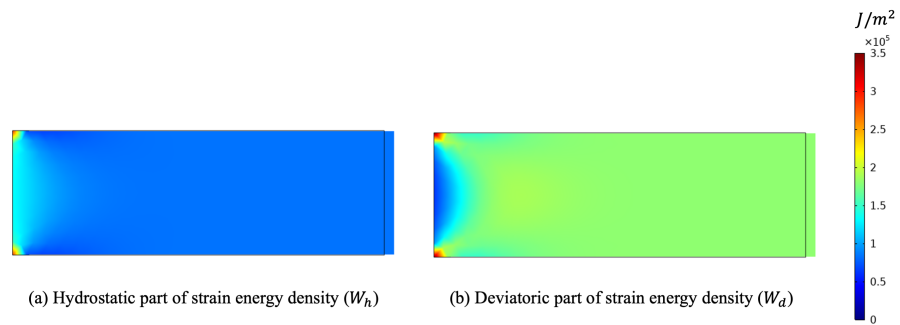


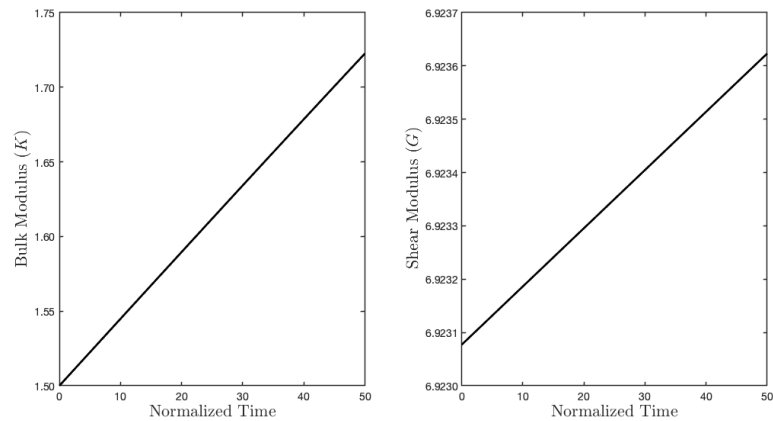
Figure 9. Schematic for the tensile test under a uniform load q_0 .



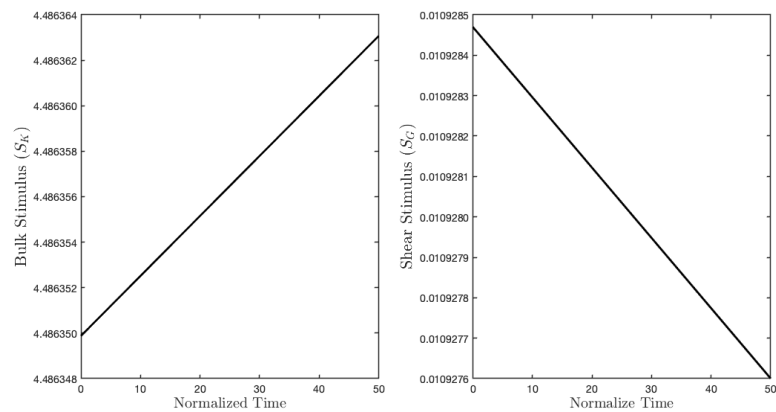
(a) Hydrostatic part of strain energy density (W_h)

(b) Deviatoric part of strain energy density (W_d)

Figure 10. Deformed shape for the tensile test (plots were obtained with a scale factor of 5).



(a) Evolution of the bulk and shear moduli, expressed in Pa.



(b) Evolution of the bulk and shear stimulus, expressed in N.

Figure 11. Evolution of moduli and stimuli in time for the tensile test.

The two kinds of deformations are almost always present in real applications, but their effects are expected to produce different outcomes. Indeed, due to the diverse nature of the material parameters involved in the evolution, one could associate their changes with various aspects. For instance, the modification in the apparent mass density is directly linked with the bulk stiffness K since a change in the porosity has a relevant effect on the hydrostatic response of the bone tissue (see, for a similar line of reasoning, the Appendix of [77]). On the other hand, the shear stiffness G is more responsible for the mechanical capability of the bone tissue to resist distortion deformations; therefore, a change in it will result in a different strength of the tissue associated with this type of deformation.

4. Conclusions

The main goal of this article was to develop a mathematical model that adequately describes the influence of hydrostatic and deviatoric loads on bone adaptation. The presented numerical simulations confirmed that the formulated mathematical description makes it possible to determine changes in bone stiffnesses, taking into account the nature of the different mechanical stimuli. It is well known that the influence of the deviatoric part is much more significant than the influence of the hydrostatic part on the magnitude of the transmitted signal and its impact on the actual bone transformation. The proposed model is able to capture this feature quite easily by changing independently a few material parameters that are responsible for the evolution of the mechanical stiffnesses, namely the ratios of the changing of the two parameters considered. This is in line with the knowledge to date regarding the function of osteocytes, which are most sensitive to flow shear loads and less to pure compression.

In future works, we plan to generalize the proposed approach to the case of orthotropic materials by introducing suitable stimuli for the evolution of each stiffnesses of the material. Indeed, the orthotropic hypothesis is more accurate in describing the mechanical behavior of a larger class of bone tissues [78,79]. However, in this work, we simplified the formulation because we believe that, especially when complex systems are to be studied, a practical approach is to explore different aspects involved in the phenomenon separately to understand their nature and develop an accurate model putting together all the insights obtained in the intermediate steps.

Author Contributions: Conceptualization, N.B., M.E.Y., A.C. and I.G.; methodology, N.B., M.E.Y., A.C. and I.G.; software, N.B.; validation, N.B., M.E.Y., A.C. and I.G.; formal analysis and investigation, N.B., M.E.Y., A.C. and I.G.; writing—original draft preparation, N.B.; writing—review and editing, M.E.Y., A.C. and I.G.; supervision, I.G. All authors have read and agreed to the published version of the manuscript.

Funding: A.C. was funded by the PON AIM grant number AIM1894130-3.

Institutional Review Board Statement: Not applicable.

Informed Consent Statement: Not applicable.

Data Availability Statement: Not applicable.

Conflicts of Interest: The authors declare no conflict of interest.

References

1. Turner, C.H. Three rules for bone adaptation to mechanical stimuli. *Bone* **1998**, *23*, 399–407. [[CrossRef](#)]
2. Li, M.C.M.; Chow, S.K.H.; Wong, R.M.Y.; Qin, L.; Cheung, W.H. The role of osteocytes-specific molecular mechanism in regulation of mechanotransduction—a systematic review. *J. Orthop. Transl.* **2021**, *29*, 1–9. [[CrossRef](#)] [[PubMed](#)]
3. Kennedy, O.D.; Laudier, D.M.; Majeska, R.J.; Sun, H.B.; Schaffler, M.B. Osteocyte apoptosis is required for production of osteoclastogenic signals following bone fatigue in vivo. *Bone* **2014**, *64*, 132–137. [[CrossRef](#)] [[PubMed](#)]
4. Klein-Nulend, J.; Bakker, A.D.; Bacabac, R.G.; Vatsa, A.; Weinbaum, S. Mechanosensation and transduction in osteocytes. *Bone* **2013**, *54*, 182–190. [[CrossRef](#)] [[PubMed](#)]
5. Kollmannsberger, P.; Kerschnitzki, M.; Repp, F.; Wagermaier, W.; Weinkamer, R.; Fratzl, P. The small world of osteocytes: Connectomics of the lacuno-canalicular network in bone. *New J. Phys.* **2017**, *19*, 073019. [[CrossRef](#)]

6. Heino, T.J.; Hentunen, T.A.; Väänänen, H.K. Conditioned medium from osteocytes stimulates the proliferation of bone marrow mesenchymal stem cells and their differentiation into osteoblasts. *Exp. Cell Res.* **2004**, *294*, 458–468. [[CrossRef](#)]
7. Bonewald, L.F. The amazing osteocyte. *J. Bone Miner. Res.* **2011**, *26*, 229–238. [[CrossRef](#)]
8. Donahue, H. Gap junctions and biophysical regulation of bone cell differentiation. *Bone* **2000**, *26*, 417–422. [[CrossRef](#)]
9. Qin, L.; Liu, W.; Cao, H.; Xiao, G. Molecular mechanosensors in osteocytes. *Bone Res.* **2020**, *8*, 1–24. [[CrossRef](#)]
10. Civitelli, R. Cell–cell communication in the osteoblast/osteocyte lineage. *Arch. Biochem. Biophys.* **2008**, *473*, 188–192. [[CrossRef](#)]
11. Weinbaum, S.; Cowin, S.C.; Zeng, Y. A model for the excitation of osteocytes by mechanical loading-induced bone fluid shear stresses. *J. Biomech.* **1994**, *27*, 339–360. [[CrossRef](#)]
12. Bakker, A.; Klein-Nulend, J.; Burger, E. Shear stress inhibits while disuse promotes osteocyte apoptosis. *Biochem. Biophys. Res. Commun.* **2004**, *320*, 1163–1168. [[CrossRef](#)] [[PubMed](#)]
13. Riddle, R.C.; Donahue, H.J. From streaming-potentials to shear stress: 25 years of bone cell mechanotransduction. *J. Orthop. Res.* **2009**, *27*, 143–149. [[CrossRef](#)] [[PubMed](#)]
14. Adachi, T.; Kameo, Y.; Hojo, M. Trabecular bone remodelling simulation considering osteocytic response to fluid-induced shear stress. *Philos. Trans. R. Soc. A Math. Phys. Eng. Sci.* **2010**, *368*, 2669–2682. [[CrossRef](#)]
15. Klein-Nulend, J.; Van Der Plas, A.; Semeins, C.M.; Ajubi, N.E.; Erangos, J.A.; Nijweide, P.J.; Burger, E.H. Sensitivity of osteocytes to biomechanical stress in vitro. *FASEB J.* **1995**, *9*, 441–445. [[CrossRef](#)] [[PubMed](#)]
16. Schaffler, M.B.; Cheung, W.Y.; Majeska, R.; Kennedy, O. Osteocytes: Master orchestrators of bone. *Calcif. Tissue Int.* **2014**, *94*, 5–24. [[CrossRef](#)] [[PubMed](#)]
17. Hadjidakis, D.J.; Androulakis, I.I. Bone remodeling. *Ann. N. Y. Acad. Sci.* **2006**, *1092*, 385–396. [[CrossRef](#)]
18. Raggatt, L.J.; Partridge, N.C. Cellular and molecular mechanisms of bone remodeling. *J. Biol. Chem.* **2010**, *285*, 25103–25108. [[CrossRef](#)]
19. Eriksen, E.F. Cellular mechanisms of bone remodeling. *Rev. Endocr. Metab. Disord.* **2010**, *11*, 219–227. [[CrossRef](#)]
20. Robling, A.G.; Castillo, A.B.; Turner, C.H. Biomechanical and molecular regulation of bone remodeling. *Annu. Rev. Biomed. Eng.* **2006**, *8*, 455–498. [[CrossRef](#)]
21. Wolff, J. Das gesetz der transformation der knochen. *Dtsch. Med. Wochenschr.* **1893**, *19*, 1222–1224. [[CrossRef](#)]
22. Wolff, J. *The Law of Bone Remodelling*; Springer Science & Business Media: Berlin/Heidelberg, Germany, 2012.
23. Pawlikowski, M.; Klasztorny, M.; Skalski, K. Studies on constitutive equation that models bone tissue. *Acta Bioeng. Biomech.* **2008**, *10*, 39–47. [[PubMed](#)]
24. George, D.; Allena, R.; Remond, Y. A multiphysics stimulus for continuum mechanics bone remodeling. *Math. Mech. Complex Syst.* **2018**, *6*, 307–319. [[CrossRef](#)]
25. George, D.; Allena, R.; Remond, Y. Integrating molecular and cellular kinetics into a coupled continuum mechanobiological stimulus for bone reconstruction. *Contin. Mech. Thermodyn.* **2019**, *31*, 725–740. [[CrossRef](#)]
26. George, D.; Allena, R.; Bourzac, C.; Pallu, S.; Bensidhoum, M.; Portier, H.; Rémond, Y. A new comprehensive approach for bone remodeling under medium and high mechanical load based on cellular activity. *Math. Mech. Complex Syst.* **2020**, *8*, 287–306. [[CrossRef](#)]
27. Bednarczyk, E.; Lekszycki, T. Evolution of bone tissue based on angiogenesis as a crucial factor: New mathematical attempt. *Math. Mech. Solids* **2022**, *27*, 976–988. [[CrossRef](#)]
28. Hernandez-Rodriguez, Y.; Lekszycki, T. Finite memory model of bone healing in analysis of moving interface between mandible tissue and bone substitute material after tooth implant application. *Contin. Mech. Thermodyn.* **2021**, 1–8. [[CrossRef](#)]
29. Hambli, R. Connecting mechanics and bone cell activities in the bone remodeling process: An integrated finite element modeling. *Front. Bioeng. Biotechnol.* **2014**, *2*, 6. [[CrossRef](#)]
30. Barkaoui, A.; Kahla, R.B.; Merzouki, T.; Hambli, R. Numerical simulation of apparent density evolution of trabecular bone under fatigue loading: Effect of bone initial properties. *J. Mech. Med. Biol.* **2019**, *19*, 1950041. [[CrossRef](#)]
31. Lekszycki, T.; dell’Isola, F. A mixture model with evolving mass densities for describing synthesis and resorption phenomena in bones reconstructed with bio-resorbable materials. *ZAMM-J. Appl. Math. Mech./Z. Angew. Math. Mech.* **2012**, *92*, 426–444. [[CrossRef](#)]
32. Prendergast, P.; Taylor, D. Prediction of bone adaptation using damage accumulation. *J. Biomech.* **1994**, *27*, 1067–1076. [[CrossRef](#)]
33. Martínez-Reina, J.; Reina, I.; Domínguez, J.; García-Aznar, J. A bone remodelling model including the effect of damage on the steering of BMUs. *J. Mech. Behav. Biomed. Mater.* **2014**, *32*, 99–112. [[CrossRef](#)] [[PubMed](#)]
34. Sheidaei, A.; Kazempour, M.; Hasanabadi, A.; Nosouhi, F.; Pithioux, M.; Baniassadi, M.; Rémond, Y.; George, D. Influence of bone microstructure distribution on developed mechanical energy for bone remodeling using a statistical reconstruction method. *Math. Mech. Solids* **2019**, *24*, 3027–3041. [[CrossRef](#)]
35. Carter, D.; Van der Meulen, M.; Beaupre, G. Mechanical factors in bone growth and development. *Bone* **1996**, *18*, S5–S10. [[CrossRef](#)]
36. Doblaré, M.; Garcia, J. Anisotropic bone remodelling model based on a continuum damage-repair theory. *J. Biomech.* **2002**, *35*, 1–17. [[CrossRef](#)]
37. Hegedus, D.; Cowin, S. Bone remodeling II: Small strain adaptive elasticity. *J. Elast.* **1976**, *6*, 337–352. [[CrossRef](#)]
38. Carter, D.; Fyhrie, D.P.; Whalen, R. Trabecular bone density and loading history: Regulation of connective tissue biology by mechanical energy. *J. Biomech.* **1987**, *20*, 785–794. [[CrossRef](#)]

39. Carter, D.; Orr, T.; Fyhrie, D.P. Relationships between loading history and femoral cancellous bone architecture. *J. Biomech.* **1989**, *22*, 231–244. [\[CrossRef\]](#)
40. Andreaus, U.; Colloca, M.; Iacoviello, D. Optimal bone density distributions: Numerical analysis of the osteocyte spatial influence in bone remodeling. *Comput. Methods Programs Biomed.* **2014**, *113*, 80–91. [\[CrossRef\]](#)
41. Lu, Y.; Lekszycki, T. New description of gradual substitution of graft by bone tissue including biomechanical and structural effects, nutrients supply and consumption. *Contin. Mech. Thermodyn.* **2018**, *30*, 995–1009. [\[CrossRef\]](#)
42. Giorgio, I.; Andreaus, U.; dell’Isola, F.; Lekszycki, T. Viscous second gradient porous materials for bones reconstructed with bio-resorbable grafts. *Extrem. Mech. Lett.* **2017**, *13*, 141–147. [\[CrossRef\]](#)
43. Andreaus, U.; Colloca, M.; Iacoviello, D. Modeling of trabecular architecture as result of an optimal control procedure. In *Biomedical Imaging and Computational Modeling in Biomechanics*; Springer: Berlin/Heidelberg, Germany, 2013; pp. 19–37.
44. Andreaus, U.; Colloca, M.; Iacoviello, D. An optimal control procedure for bone adaptation under mechanical stimulus. *Control Eng. Pract.* **2012**, *20*, 575–583. [\[CrossRef\]](#)
45. Giorgio, I.; Andreaus, U.; Alzahrani, F.; Hayat, T.; Lekszycki, T. On mechanically driven biological stimulus for bone remodeling as a diffusive phenomenon. *Biomech. Model. Mechanobiol.* **2019**, *18*, 1639–1663. [\[CrossRef\]](#) [\[PubMed\]](#)
46. Lekszycki, T. Functional adaptation of bone as an optimal control problem. *J. Theor. Appl. Mech.* **2005**, *43*, 555–574.
47. Reda, H.; Karathanasopoulos, N.; Elnady, K.; Ganghoffer, J.F.; Lakiss, H. The role of anisotropy on the static and wave propagation characteristics of two-dimensional architected materials under finite strains. *Mater. Des.* **2018**, *147*, 134–145. [\[CrossRef\]](#)
48. Ganghoffer, J.; Reda, H. A variational approach of homogenization of heterogeneous materials towards second gradient continua. *Mech. Mater.* **2021**, *158*, 103743. [\[CrossRef\]](#)
49. Reda, H.; Rahali, Y.; Ganghoffer, J.; Lakiss, H. Wave propagation analysis in 2D nonlinear hexagonal periodic networks based on second order gradient nonlinear constitutive models. *Int. J. Non-Linear Mech.* **2016**, *87*, 85–96. [\[CrossRef\]](#)
50. Massoumi, S.; La Valle, G. Static analysis of 2D micropolar model for describing granular media by considering relative rotations. *Mech. Res. Commun.* **2022**, *119*, 103812. [\[CrossRef\]](#)
51. La Valle, G.; Massoumi, S. A new deformation measure for micropolar plates subjected to in-plane loads. *Contin. Mech. Thermodyn.* **2022**, *34*, 243–257. [\[CrossRef\]](#)
52. Belarbi, M.O.; Li, L.; Houari, M.S.A.; Garg, A.; Chalak, H.D.; Dimitri, R.; Tornabene, F. Nonlocal vibration of functionally graded nanoplates using a layerwise theory. *Math. Mech. Solids* **2022**. [\[CrossRef\]](#)
53. Karamooz Ravari, M.; Kadkhodaei, M. A computationally efficient modeling approach for predicting mechanical behavior of cellular lattice structures. *J. Mater. Eng. Perform.* **2015**, *24*, 245–252. [\[CrossRef\]](#)
54. Barchiesi, E.; dell’Isola, F.; Bersani, A.M.; Turco, E. Equilibria determination of elastic articulated duoskelion beams in 2D via a Riks-type algorithm. *Int. J. Non-Linear Mech.* **2021**, *128*, 103628. [\[CrossRef\]](#)
55. Cazzani, A.; Stochino, F.; Turco, E. An analytical assessment of finite element and isogeometric analyses of the whole spectrum of Timoshenko beams. *ZAMM-J. Appl. Math. Mech./Z. Angew. Math. Mech.* **2016**, *96*, 1220–1244. [\[CrossRef\]](#)
56. Turco, E.; Barchiesi, E.; dell’Isola, F. In-plane dynamic buckling of duoskelion beam-like structures: discrete modeling and numerical results. *Math. Mech. Solids* **2021**. [\[CrossRef\]](#)
57. Pietraszkiewicz, W.; Eremeyev, V. On natural strain measures of the non-linear micropolar continuum. *Int. J. Solids Struct.* **2009**, *46*, 774–787. [\[CrossRef\]](#)
58. Eremeyev, V.A.; Pietraszkiewicz, W. Material symmetry group and constitutive equations of micropolar anisotropic elastic solids. *Math. Mech. Solids* **2016**, *21*, 210–221. [\[CrossRef\]](#)
59. Misra, A.; Poorsolhjouy, P. Identification of higher-order elastic constants for grain assemblies based upon granular micromechanics. *Math. Mech. Complex Syst.* **2015**, *3*, 285–308. [\[CrossRef\]](#)
60. De Angelo, M.; Placidi, L.; Nejadi Sadeghi, N.; Misra, A. Non-standard Timoshenko beam model for chiral metamaterial: identification of stiffness parameters. *Mech. Res. Commun.* **2020**, *103*, 103462. [\[CrossRef\]](#)
61. Abali, B.E.; Müller, W.H.; Eremeyev, V.A. Strain gradient elasticity with geometric nonlinearities and its computational evaluation. *Mech. Adv. Mater. Mod. Process.* **2015**, *1*, 1–11. [\[CrossRef\]](#)
62. Abali, B.E.; Müller, W.H. Theory and computation of higher gradient elasticity theories based on action principles. *Arch. Appl. Mech.* **2017**, *87*, 1495–1510. [\[CrossRef\]](#)
63. Cuomo, M.; dell’Isola, F.; Greco, L.; Rizzi, N. First versus second gradient energies for planar sheets with two families of inextensible fibres: Investigation on deformation boundary layers, discontinuities and geometrical instabilities. *Compos. Part B Eng.* **2017**, *115*, 423–448. [\[CrossRef\]](#)
64. Eugster, S.R.; dell’Isola, F.; Fedele, R.; Seppecher, P. Piola transformations in second-gradient continua. *Mech. Res. Commun.* **2022**, *120*, 103836. [\[CrossRef\]](#)
65. dell’Isola, F.; Eugster, S.R.; Fedele, R.; Seppecher, P. Second-gradient continua: From Lagrangian to Eulerian and back. *Math. Mech. Solids* **2022**. [\[CrossRef\]](#)
66. Spagnuolo, M.; Franciosi, P.; dell’Isola, F. A Green operator-based elastic modeling for two-phase pantographic-inspired bi-continuous materials. *Int. J. Solids Struct.* **2020**, *188*, 282–308. [\[CrossRef\]](#)
67. Solyaev, Y.; Lurie, S.; Altenbach, H.; dell’Isola, F. On the elastic wedge problem within simplified and incomplete strain gradient elasticity theories. *Int. J. Solids Struct.* **2022**, 239–240, 111433. [\[CrossRef\]](#)
68. Laudato, M.; Ciallella, A. Perspectives in generalized continua. In *Developments and Novel Approaches in Biomechanics and Metamaterials*; Springer: Berlin/Heidelberg, Germany, 2020; pp. 1–13.

69. Andreaus, U.; Spagnuolo, M.; Lekszycki, T.; Eugster, S.R. A Ritz approach for the static analysis of planar pantographic structures modeled with nonlinear Euler–Bernoulli beams. *Contin. Mech. Thermodyn.* **2018**, *30*, 1103–1123. [[CrossRef](#)]
70. Barchiesi, E.; Eugster, S.R.; dell’Isola, F.; Hild, F. Large in-plane elastic deformations of bi-pantographic fabrics: asymptotic homogenization and experimental validation. *Math. Mech. Solids* **2020**, *25*, 739–767. [[CrossRef](#)]
71. dell’Isola, F.; Andreaus, U.; Placidi, L. At the origins and in the vanguard of peridynamics, non-local and higher-gradient continuum mechanics: An underestimated and still topical contribution of Gabrio Piola. *Math. Mech. Solids* **2015**, *20*, 887–928. [[CrossRef](#)]
72. Yang, Z.; Oterkus, E.; Nguyen, C.T.; Oterkus, S. Implementation of peridynamic beam and plate formulations in finite element framework. *Contin. Mech. Thermodyn.* **2019**, *31*, 301–315. [[CrossRef](#)]
73. Oterkus, S.; Madenci, E.; Oterkus, E. Fully coupled poroelastic peridynamic formulation for fluid-filled fractures. *Eng. Geol.* **2017**, *225*, 19–28. [[CrossRef](#)]
74. Pisano, A.A.; Fuschi, P. Structural symmetry within nonlocal integral elasticity: theoretical issues and computational strategies. *Curved Layer. Struct.* **2017**, *4*, 1–7. [[CrossRef](#)]
75. Mullender, M.; Huiskes, R.; Weinans, H. A physiological approach to the simulation of bone remodeling as a self-organizational control process. *J. Biomech.* **1994**, *27*, 1389–1394. [[CrossRef](#)] [[PubMed](#)]
76. Lekszycki, T. Modelling of bone adaptation based on an optimal response hypothesis. *Meccanica* **2002**, *37*, 343–354. [[CrossRef](#)]
77. Andreaus, U.; Giorgio, I.; Madeo, A. Modeling of the interaction between bone tissue and resorbable biomaterial as linear elastic materials with voids. *Z. Angew. Math. Phys.* **2015**, *66*, 209–237. [[CrossRef](#)]
78. Allena, R.; Cluzel, C. Heterogeneous directions of orthotropy in three-dimensional structures: Finite element description based on diffusion equations. *Math. Mech. Complex Syst.* **2018**, *6*, 339–351. [[CrossRef](#)]
79. Cluzel, C.; Allena, R. A general method for the determination of the local orthotropic directions of heterogeneous materials: Application to bone structures using μ CT images. *Math. Mech. Complex Syst.* **2018**, *6*, 353–367. [[CrossRef](#)]